SAND2022-5154C

Proceedings of the ASME 2022 Heat Transfer Summer Conference
SHTC2022
July 11 – 13, 2022, Philadelphia, Pennsylvania

SHTC2022-79560

CHARACTERIZATION OF VENTED GAS PREDICTIONS IN LITHIUM-ION MODELING WITH 1-D THERMAL RUNAWAY (LIM1TR)

Ala' E. Qatramez[1], Andrew Kurzawski[2],John Hewson[2],
Michael Parker[1], Adam Porter[1],Daniel Foti[1], Alexander J. Headley[1,*]
[1]Department of Mechanical Engineering, University of Memphis, Memphis, Tennessee, 38152
[2]Fire Science and Technology Department, Sandia National Laboratories, Albuquerque, New Mexico, 87185

ABSTRACT

Thermal runaway and its propagation are major safety issues in containerized lithium-ion battery energy storage systems. While conduction-driven propagation has received much attention, the thermal hazards associated with propagation via hot gases vented from failing cells are still not fully understood. Vented gases can lead to global safety issues in containerized systems, via heat transfer to other parts of the system and potential combustion hazards. In this work, we validate the characteristics of vented gases from cells undergoing thermal runaway in the thermal propagation model LIM1TR (Lithium-ion Modeling with 1-D Thermal Runaway). In particular, we assess the evolution of vented gases, venting time, and temperature profiles of single cell and multi-cell arrays based on experiments performed in Archibald et al *(Fire Technology, 2020). While several metrics for estimating the venting time are assessed, a metric based on the CO_2 generation results in consistent predictions. Vented gas evolution, and venting times predicted by the simulations are consistent with those estimated during the experiments. The simulation resolution and other model parameters, especially the use of an intra-particle diffusion limiter, have a large role in prediction of venting time.*

1 Introduction

The need for grid-scale energy storage systems (ESSs) is increasing as renewable energy utilization expands. The unique characteristics of Lithium-ion batteries (LIBs), such as their high energy density, high efficiency, load flexibility and relative maturity, have made them the front runner for grid-scale energy storage thus far. However, serious safety issues are associated with these ESSs as a significant amount of energy is stored in relatively small spaces. One of these safety concerns is thermal runaway of LIBs.

Thermal runaway occurs when a LIB is subjected to abnormal conditions, such as thermal abuse or overheating, mechanical or electrical events [1–3], which induce uncontrolled reactions between the battery materials. During thermal runaway hot, combustible gases are produced from the reactions and are vented out of the battery cell. The rate of venting depends on many factors such as the cell materials, state of charge, the cause of thermal runaway [4], and cell temperature. A significant amount of thermal and chemical energy is stored in the vented gases. If a battery undergoes thermal runaway in a containerized ESS, there is a major concern that heat can propagate to other battery modules via the vented products and compromise the safety of the entire system. For example, in April 2019, an explosion of vented gas products in a LIB energy storage facility in Arizona resulted in serious injuries [5]. In September 2021, in California, an overheating incident was reported in Phase 1 of the Vistra's Moss Landing Energy Storage Facility, currently the largest battery storage facility in the world [6]. Furthermore, more than 30 ESS fires causing considerable financial loss were reported in South Korea as of August 2021 [7].

Numerous numerical and experimental studies [8–12] have investigated how to mitigate the propagation of thermal runaway caused by heat conduction between adjacent cells. The propagation of thermal runaway of an entire module was studied experimentally for cylindrical 18650 cells and pouch cells [8]. The

*Email address for correspondence: jheadley@memphis.edu

results of these experiments showed that the gap between cylindrical cells plays a major role in limiting heat transfer from a failed cell to neighboring cells and therefore limits thermal runaway propagation. While the large direct contact area between pouch cells increases the chance of thermal runaway propagation, thermal insulation between cells can play a significant role in preventing propagation. Ref. [9] shows that heat transfer from a failed cell can be reduced by installing metal plates of different materials and thicknesses between cells. The results show that plates with sufficient heat capacity were able to prevent propagation entirely, while ones with small thickness only mitigated propagation.

However, few experiments have investigated the characteristics of vented gases during thermal runaway. Archibald *et al* [13] performed experiments on 5 Ah and 10 Ah cells to study failure of pouch LIB cells due to (1) direct external heating and (2) thermal runaway propagation from adjacent cells, as well as the characteristics of these two different types of failure. Their experiments showed that thermal runaway induced by direct heating took longer than by propagation [13]. Such work builds the foundation for understanding thermal propagation by the vented gases in containerized ESSs, but more investigation is needed to further assess the potential hazards and mitigation strategies.

The goal of this work is to validate the ability of LIM1TR (Lithium-ion Modeling with 1-D Thermal Runaway), a LIB thermal propagation model developed at Sandia National Laboratories [14,15], to predict vented gases characteristics produced during thermal runaway. The results of this modeling effort will be validated using single cell and array experiments of 5 Ah LIB cells conducted in Ref. [13]. Here we investigate the effect of the time step used for the conduction model (Δt), the number of control volumes (N), and the use of a reaction limiting model [16] on simulated vented gas characteristics. We will assess (1) the total moles of gas produced, (2) temperature measurements, and (3) the venting time. Selection of input parameters of LIM1TR will be addressed. This work helps to lay the groundwork for further investigations of vented gas hazards for a wide array of LIB sizes and configurations.

2 Methodology

For this effort, single and five-cell array 5 Ah LIB experiments from [13] were used to validate LIM1TR simulations. To achieve agreement between the simulations and experiments, the modeling parameters had to be carefully considered. In the following section, we will describe the experiments used for validation and discuss key modeling considerations, such as heating times, boundary conditions, and spatial/temporal discretization.

2.1 Validation Experiment Summary

The experiments used for validation were performed in a sealed pressure vessel. All of the experiments referenced here used 5 Ah cells that were 75.5 mm $\times$ 64.5 mm $\times$ 9.0 mm. However, there were some key differences between the single cell and array experiments that may have led to significant differences in the cell failures.

Firstly, in the single cell experiments, a heater on each side of the cell were used to initiate thermal runaway. These two heaters were inserted in aluminum blocks to distribute the heat evenly on the sides of the cell. The remaining perimeter of cell was insulated with ceramic fiber. Conversely, for the multi-cell array experiments, a single heater was centered on the side of the first cell in the array to initiate thermal runaway on that cell and then propagate to successive cells via conduction [13].

Secondly, for the single cell experiments the cell was heated at a constant rate of 5 °C/min to cause the failure, while in the case of the array experiments it was heated at a rate of up to 100 °C/min until thermal runaway began. For single cell experiments, the beginning of the thermal runaway event was identified by a heating rate (dT/dt) in excess of 100 °C/s measured between the heater and failing cell. These heating rates resulted in significantly different surface temperatures when thermal runaway began, between 185 and 196 °C for single cell experiments, and between 400 °C and 500 °C for the array experiments [13].

All of these particulars required consideration when determining the best parameters for the simulations as will be discussed further in the following section.

2.2 LIM1TR

In this work, LIM1TR was used to simulate thermal runaway and make predictions of the heat and gas generated from failing cells. LIM1TR is an open-source software that employs a finite volume method and temporal operator splitting to solve the heat equation with chemical source terms on a quasi-1D domain [14]. This formulation captures conduction heat transfer in one direction along a stack of cells and/or inert materials as well as heat transfer to the surroundings through an applied flux or convective boundary condition. The heat equation can be written as

$$\rho c_p \frac{\partial T}{\partial t} = \nabla.(k\nabla T) + \dot{q}''', \tag{1}$$

where ρ is the cell density in kg/m^3, and c_p and k are the specific heat and thermal conductivity of the cell in J/kgK and W/mK, respectively. While $\dot{q}'''$ is the source volumetric heat in W/m^3 due to reactions in the cell. More details on the model formulation can be found in Ref. [14].

For the following simulations, a three-reaction mechanism was modeled in LIM1TR representing three important reactions

in LIB thermal runaway; 1) SEI decomposition [17], 2) anode-electrolyte reactions [18,19], and 3) cathode-electrolyte reactions [20–22]. Details of the reaction system can be found in Ref. [16]. These reactions convert active electrode materials and electrolyte to solid and gaseous products.

The global reactions for the SEI decomposition, anode-electrolyte reactions, and cathode-electrolyte reactions are shown below, respectively:

$$\begin{aligned} (CH_2OCO_2Li)_2 &\longrightarrow Li_2CO_3 + C_2H_4 + CO_2 + \frac{1}{2}O_2, \\ 2C_6Li + C_3H_4O_3 &\longrightarrow 2C_6 + Li_2CO_3 + C_2H_4, \\ 5CoO_2 + C_3H_4O_3 &\longrightarrow 5CoO + 3CO_2 + 2H_2O. \end{aligned} \tag{2}$$

In addition to the global reactions, an intra-particle diffusion limiter as implemented in Ref. [16] was included in the anode-electrolyte and cathode-electrolyte reactions. This model considers the diffusion of lithium and oxygen through the anode and cathode particles, respectively. When matched in serial with the electrolyte reactions at the surface of the particles, the reaction rate takes the form $k_j/(1+Da_j)$, where the subscript "j" indexes the anode and cathode reactions. The Damköhler number has the form:

$$Da_j = \frac{aA_j \exp\left(-\frac{E_j}{RT}\right)(r_o - r_i)\, r_o}{a_p \rho D_{0,j} \exp\left(-\frac{E_{D,j}}{RT}\right) r_i}, \tag{3}$$

which describes the ratio of the electrode-electrolyte reaction rate to the intra-particle diffusion rate through a spherical shell with inner radius r_i and outer radius r_o. At high temperatures, the propagation of thermal runaway becomes controlled by diffusion as the Damköhler number becomes larger. This will be referred to as the Damköhler limiter model (DLM) in the following sections. More details on this model can be found in Ref. [16].

This multi-physics model combines both the conduction and combustion mechanisms, allowing for simulation of reaction front propagation through LIBs in 1D if the correct boundary conditions and parameters are used. The importance of the modeling parameters will be shown in the following sections.

It should be noted, however, that there are some potential physics that will occur in actual thermal runaway events that are not captured in the following simulations. For instance, separator melting can occur at thermal runaway temperatures, leading to additional short circuit reactions that also release heat. These short-circuit reactions are not included in the present simulations because the heating rates associated with the anode and cathode reactions are much larger than those from short circuits under these conditions. Further, LIM1TR does not currently include an explicit model for electrolyte venting during thermal runaway. Direct electrolyte venting can help in capturing the dynamics of material loss during thermal runaway as shown by Coman *et al* [23], who modeled the vented electrolyte as ideal gas flows through an orifice. In the current simulations, the electrolyte concentration available to react with the electrodes was reduced to match the observed heat release in lieu of a venting model.

2.3 Single Cell Simulation Input

To model the experiments accurately, the size of the cell, heating methods, heating rate and heating duration should be set to reflect the experiment as closely as possible. For the single cell experiments, the cells were sandwiched between two 0.5" aluminum plates as shown in Fig. 1. For the simulations, a heat flux of 3650 W/m^2 was distributed over sides of the aluminum plates for 1700 s to approximate the heating rate and duration measured in the experiments. A convection coefficient of 5 W/m^{2}K was used on the external surfaces of the cell (see Fig. 1). The two aluminum plates were discretized as 20 control volumes ($N = 20$). The initial cell temperature and outside temperature were set to be 25 °C for all the simulations.

2.4 Five-Cell Array Simulation Input

To match the heating condition in the array experiment, a heat flux of 5050 W/m^2 is applied to the first cell for 650 s. Though the exact heating duration for the experiment was not reported, thermal runaway of the first cell occurred before 700 s. Insulation was only modeled after the last cell in the array in the simulation so the heat flux could be applied to the cell directly. A convective boundary condition with convection coefficient of 10 W/m^{2}K is used on the external cell faces. This is higher than the one used for the single cell simulation, because the single cell experiments use insulation on the external faces. Insulation with a specific heat of 819.4 J/kgK was modeled on the right side of the cell array ($N = 4$). This was chosen based on the value of calcium silicate board measured in Ref. [24] to give a thermal diffusivity on the order of 10^{-7}. A convection coefficient of 5 W/m^{2}K is used on the right side of the insulation similarly to the single cell simulations. This combination of boundary conditions was selected to to emulate the cooling rate seen after the runaway events in the experiments.

3 Results

A parametric study with forty-five simulations of the single cell and the five-cell 5 Ah array cases was performed by changing the simulation time step, Δt, number of control volumes in the cell, N, and whether or not the DLM was used to study the sensitivity of simulation results to these parameters and the agreement with the experiments. Data from simulations were collected at uniform time intervals.

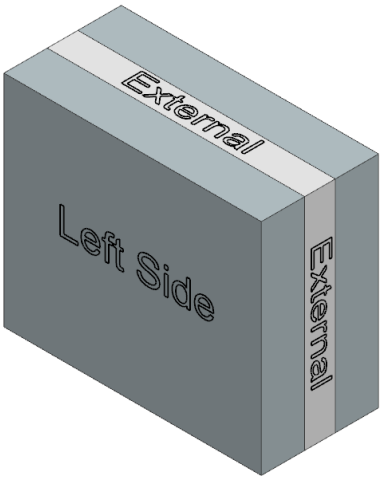

FIGURE 1. Domain table of the single cell simulations layout showing the cell and the two aluminum plates. The dimensions are to scale.

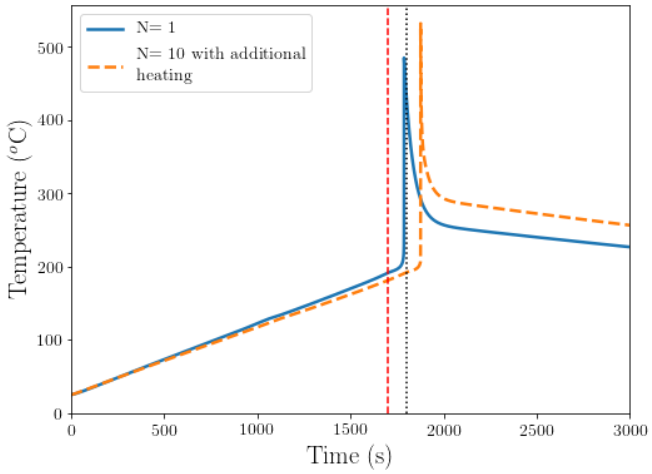

FIGURE 2. Interface temperature profile between the first aluminum plate and cell for single cell where the DLM is deactivated. The dashed line indicates the time when the heating stopped, while the dotted line shows additional 100 s of heating for N= 10 case.

3.1 Single Cell Simulations

Figure 2 shows the interface temperature profiles between the first aluminum plate and the cell when the DLM is deactivated ($\Delta t = 0.001$ and $N = 1$ and 10). The temperature response is similar regardless of the number of control volumes used, but there is small delay in the thermal runaway going from a single control volume simulation to higher resolutions. The maximum reported vented gas temperature from Ref. [13] was 900 °C, and the maximum cell temperature of the first control volume for $N = 10$ is about 840 °C without the DLM (surface temperatures shown in Fig. 2 are substantially lower because they measure the average of the cell and aluminum block). For the $N = 1$ case without the DLM, the interface temperature when the heater is turned off (before the reaction occurs) is 191.5 °C, which is in the range of measured temperature in the experiments (185 to 196 °C).

It is also important to assess the amount of gas vented during thermal runaway. The moles of vented gases from the simulation $n_{gas,sim}$ were calculated and compare with the moles of vented gas estimated from the experimental data $n_{gas,exp}$. For the simulations, the moles of gas produced can be directly calculated as from the output of the model. To compare this to the experimental results, the gas production was estimated from the changes in temperature and pressure after cell venting events during the experiments performed in a sealed pressure vessel.

Firstly, the volume of the air space in the pressure vessel was known, and the pressure and temperature before the first cell failure could be used to estimate the moles of gas in the vessel before any reaction products were vented into the vessel using the ideal gas law:

$$n_{N_2,i} = \frac{P_{exp,i} V_{vessel}}{R_u T_{exp,i}}, \tag{4}$$

where $n_{N_2,i}$ is the initial moles of nitrogen in the vessel, R_u is the universal gas constant, $P_{exp,i}$ initial pressure, and $T_{exp,i}$ is initial temperature of the gas reported in [13]. Note that [13] reported gage pressures, and an atmospheric pressure of 101.3 kPa was assumed.

To estimate the moles of gas vented from cell failures, the temperature after the venting process was used to determine the partial pressure of the nitrogen in the vessel and any pressure measured in excess of this amount was assumed to come from the vented gases. It was further assumed that the vented gases were ideal the moles of vented gas was calculated as:

$$\begin{aligned} P_{N_2,f} &= \frac{n_{N_2,i} R_u T_{exp,f}}{V_{vessel}} \\ P_{vent} &= P_{exp,f} - P_{N_2,f} \\ n_{vent} &= \frac{P_{vent} V_{vessel}}{R_u T_{exp,f}}, \end{aligned} \tag{5}$$

where $T_{exp,f}$ is the measured temperature after the venting process, $P_{exp,f}$ is the final total measured pressure, $P_{N_2,f}$ is the partial pressure of the nitrogen that was initially in the test vessel, and

P_{vent} is the partial pressure of the vented gases. This was done similarly for each cell failure for the 10 cell and 5 cell tests of 5Ah cells in [13].

Using this method, the estimated moles of vented gas per cell failure from the experiments was 0.1836 mol (σ = 0.0692 mol) for all the 5Ah cells. The simulation quantity of vented gases was in good agreement at 0.1868 mol, suggesting that the three reaction model used for these simulations gives a reasonable representation of real scenarios.

It is also important to evaluate the duration of the venting process and the temperature of the cell during and after thermal runaway to best understand the associated safety hazards. Venting time is an important characteristic of vented gases and is directly related to the reaction rate and further to the exit velocity of the gases, which is a critical parameter to assess the heat transfer from vented gases. Two approaches were used to evaluate the venting duration: a heating rate approach and a progress variable approach based on CO_2 concentration ($[CO_2]$). The heating rate was used in Ref. [13] to turn off the heater for five-cell 5 Ah array, and identify when the rapid heat release occurred for the single cell.

As an alternate method to evaluate the venting time, we also introduce the following progress variable θ:

$$\theta = \frac{[CO_2]_t - [CO_2]_{t=ref}}{[CO_2]_{max} - [CO_2]_{t=ref}}, \tag{6}$$

where $[CO_2]$ refers to the total mass of CO_2 of all control volumes in the cell, and $[CO_2]_{max}$ is the maximum CO_2 mass, and $[CO_2]_t$ is the CO_2 mass at time t. $[CO_2]_{t=ref}$ is the CO_2 mass at a reference time where there is no change of CO_2 mass since some CO_2 is produced during heating before the main reaction occurs. This reference is chosen at $t = 1200$ s for single cell and $t = 50$ s for five-cell array. This metric is dominated by the cathode reaction, since CO_2 is not a product of the anode reaction as it is shown in Eq. 2. The reaction or venting time can be defined as

$$t_{venting} = t(\theta = 0.99) - t(\theta = 0.25), \tag{7}$$

where $t(\theta = 0.99)$ is the time where θ equals 0.99 (the end of the reaction) and $t(\theta = 0.25)$ is the time where θ equals 0.25. Similarly, the venting time using the heating rate approach is defined as

$$t_{venting} = t(\frac{dT}{dt} <= 1 \times 10^{-2}) - t(\frac{dT}{dt} >= 100), \tag{8}$$

where $t(\frac{dT}{dt} >= 100$ is the time where dT/dt is equal or greater than 100 $^{\circ}$C/s, since it is the value that was used to turn off the heater for five-cell 5 Ah array and where the rapid heat release occurred for the single cell in [13], and $t(\frac{dT}{dt} <= 1 \times 10^{-2})$ is the time where dT/dt is equal or less than 10^{-2} $^{\circ}$C/s. A small value is chosen to indicate the end of the reaction since no parameter was mentioned to identify the end of the thermal runaway in the Ref. [13] for single cell. However, it is important to mention that dT/dt is directly calculated from the heating rate of the surface control volume in the simulations (see Eq.1), while it is from a thermocouple measurement in the experiments. This difference could lead to some discrepancies. Since the high heating rates from the simulations are due to chemical reactions, they are a good indicator of the start and the end of thermal runaway.

Simulations with $\Delta t = 0.01, 0.005$ and 0.001 and $N = 1, 2, 10, 30, 60$, and 90 were performed with and without activating the DLM to study the sensitivity of the venting time to these parameters. The results show that the temporal resolutions used, Δt, had no effect on the venting time for both cases. Figure 3 shows the estimated venting time for $N = 1$ and $\Delta t = 0.001$ with and without the DLM. This Figure shows that the progress variable approach estimates higher venting times than the reaction heating rate without DLM, while when employing the DLM the reaction heating rate approach estimates higher venting time than the progress variable method. So, there is a significant difference in venting times between simulations with and without the DLM, also Ref. [13] estimated about 4 s on average to capture the travel of the temperature rise form one side of the cell to other side through the thickness. To study venting time sensitivity of spatial resolutions, N, and the effect of the DLM, different spatial resolutions were tested.

To start this analysis, Figure 4(a) and Figure 4(a) show the progress variable and heating rate of the first control volume for $\Delta t = 0.01$ and 0.001, and $N = 90$ with the DLM. This Figure further shows that the Δt values used has no effect on progress variable and heating rate profiles. This is significant as increasing the temporal resolution by a factor of 10 has a major impact on the simulation time.

Simulations without the DLM were also performed to evaluate its effect on venting time estimates. The progress variable was used to identify the venting time in this case since it is hard to identify the beginning of the reaction using the heating rate approach when the DLM is deactivated. Figure 5 shows that the venting time approaches 4 s as N increases (4.5 s for $N = 90$) using the progress variable approach without the DLM. In general, as N increases the venting time converges as heat conduction through the cell is better resolved. Again, this is close to the experimentally measured venting time of 4 s. However, using the DLM led to significantly longer venting time estimates. Comparing Fig. 4 and Fig. 5, when the DLM was activated the thermal runaway became slower since longer venting time was estimated. For DLM simulations,the venting time estimated by the progress variable was $\sim$ 10-12 s, and $\sim$ 6-9 s using the heating rate approach and increasing spatial resolution led to longer

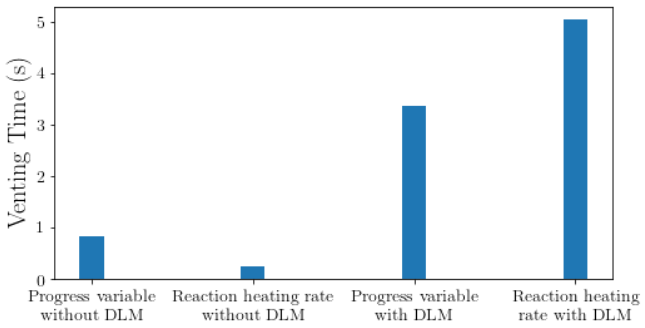

FIGURE 3. Venting time estimated by both progress variable and heating rate for N= 1 and $\Delta t = 0.001$ with/ without activating the DLM for single cell.

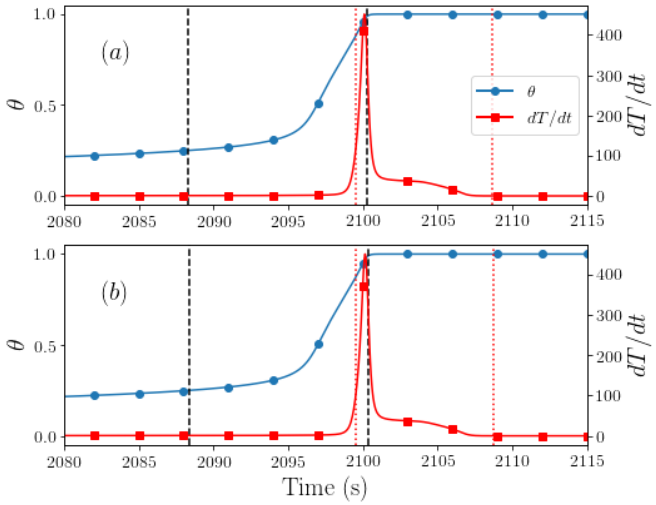

FIGURE 4. Progress variable and heating rate of the first control volume for $N = 90$, and (a) $\Delta t = 0.01$ and (b) 0.001 with activating the DLM for single cell, respectively. Dashed lines indicate the start and the end of the reaction using the progress variable approach, while dotted ones are related to heating rate approach.

venting times. This is an indication that the DLM is not effective for this scenario as it excessively limits realistic reaction rates.

Figure 5 also shows that the progress variable approach led to higher venting time estimates than the heating rate approach. This could be because of the difference in the bulk cell consideration for the progress variable approach versus the surface consideration of the heating rate approach. This makes the heating rate approach inaccurate for capturing the beginning of the reaction as the reaction was observed to start in the core of the cell for these simulations. The efficacy of the progress variable approach for reaction identification from simulations will be further expounded upon below.

To summarize the results for the single cell simulations, three major parameters were considered: the time step, spatial resolutions, and use of the DLM. It was found that the time step had no effect on the estimated venting time with the time step values investigated in this study, which indicates that the conduction time step was sufficiently resolved at 0.01 s, but the x-dimension needs to be well-resolved. This was true regardless of the venting time estimation approach used (progress variable or heating rate). To match the single cell experiments, no DLM was needed, and increasing the number of control volumes made the venting time estimates approach the experimental results. Though this was true for the single cell situation where the cell was heated on both sides, it could be significantly different for the array propagation case where heating is uneven and conduction plays a larger role. This will be discussed in the following section.

3.2 Five-Cell Array Simulations

We start the validation with temperature profiles of five-cell 5 Ah array in Ref. [13] and the simulated interface temperature profiles. The results in the first cell in the array will be studied based on the first control volume since it is the control volume that is directly in contact with the heat flux. Figure 6(a) shows the temperature profile of the first node of cell 1, the interface temperature profiles between cells, and between the last cell and the insulator for $N = 90$ with the DLM. Figure 6(b) shows the interface temperature measurements between the cells for the five-cell 5Ah array experiment in Ref. [13]. Experimental measurements in Fig. 6(b) show some high temperature bursts (T $>$ 1000 °C) that are likely representative of flaming gases from the vented gases.

Temperature profiles in Fig. 6 show that thermal runaway in the first cell begins earlier in the simulation than in the experiments, while the total simulated propagation time ($\sim$ 90 s) is longer than the experiment ($\sim$ 65 s). This is likely due to some experimental conditions being unknown, as well as some limitations in the model as it is a quasi 1-D formulation. For example, the heat flux boundary conditions in the simulations could be overestimated as we are not resolving the localized heating (center of the cell face) from the experiments in the quasi 1-D formulation (full cell face), which could have caused the first cell to undergo thermal runaway earlier. The duration to apply the heat flux boundary condition was also not known in detail from the experiments. Contact resistances between the cells and the cell thermal conductivity play critical roles in slowing and even preventing thermal runaway. By comparing the temperatures of the second and third cells before the thermal runaway occurred in Fig. 6(a) and 6(b), we can see that the contact resistance between the cells is likely underestimated or the modeled thermal conductivity is too large. The effects of these parameters could

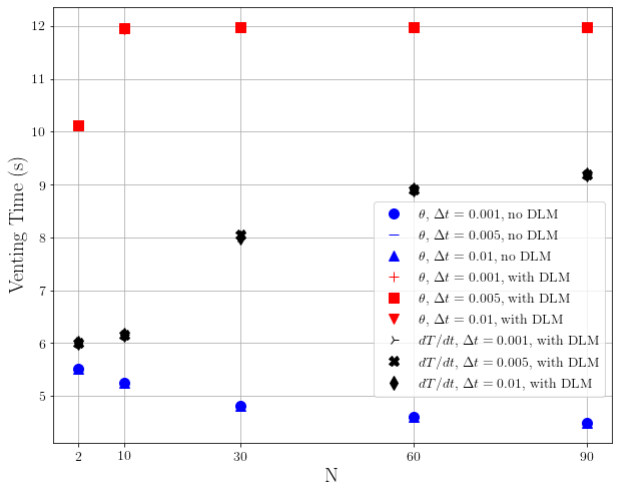

FIGURE 5. Venting time estimated for $N = 2$, 10, 30, 60, and 90 for all Δt for single cell using progress variable approach where DLM was deactivated (θ, no DLM), progress variable approach with DLM (θ, with DLM), and heating rate approach with DLM (dT/dt, with DLM).

explain thermal runaway beginning sooner in the simulations and taking longer to progress through the full stack.

To estimate the venting and heating times for each cell, gas pressure measurements were used in the experimental tests in Ref. [13]. For the following results, the progress variable approach will be used to estimate venting times as it is based on CO_2 production, which can be related directly to the gas pressure. Experimental results in Ref. [13] show that the average venting time is about 11 s, while the average preheating time is about 4 s.

Figure 7(a) and Figure 7(b) show the progress variable for simulations with and without the DLM for $N = 90$. The venting time for a given cell is estimated as the interval between the vertical dashed and solid lines that identify the beginning and end of the reaction for that cell, respectively. The preheating time is the interval between end of the reaction of a prior cell (solid line) and the beginning of the reaction of that cell (dashed line). For example, the heating time of cell 2 is the interval between the first solid line and the second dashed line. In general, Figure 7 shows that when the DLM was deactivated the thermal runaway occurred earlier and the whole stack failed in less time. The evolution of gases over the duration of stack propagation during thermal runaway from DLM and non-DLM simulations is shown in Fig. 8. As each cell goes into thermal runaway gases are generated, and successive failures add to the vented products collected in the container. Because these gases are known to be flammable [25] the overall gas generation from multiple cell failures represents

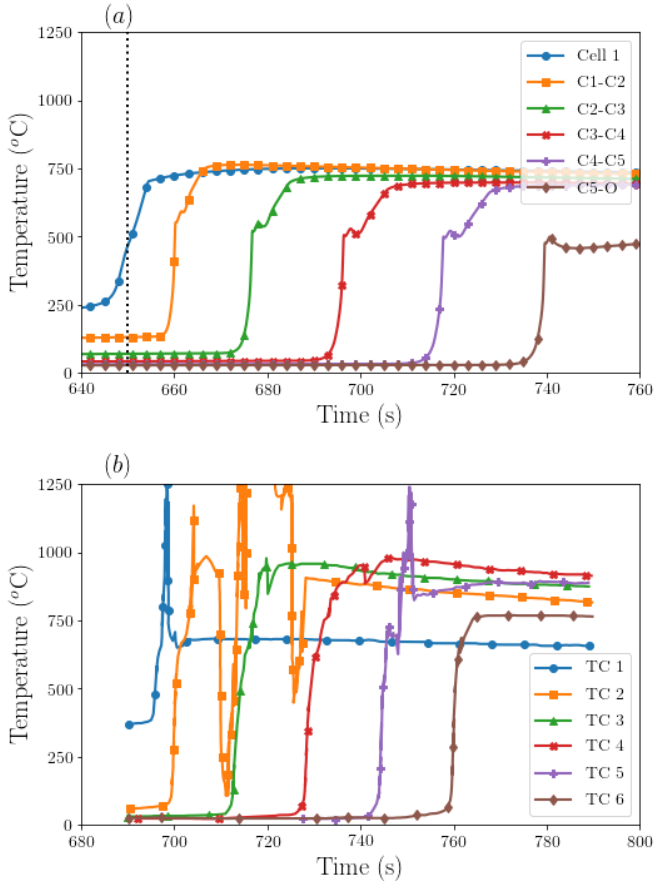

FIGURE 6. (a) Temperature profile of the first control volume of cell 1, the interface temperature profiles between cells, and between the last cell and the insulator for $N = 90$ and $\Delta t = 0.001$ with activating the DLM for five-cell array. The dotted line indicates the time when the heating stopped. (b) Interface temperature measurements between the cells for five-cell 5 Ah array experiment [13]. Both figures show the temperature profiles for 120 s interval. Figure 6(b) was reproduced with permission from Fig. 6(B) in Ref. [13]).

a significant hazard. This long term gas generation rate is significant for heat transfer concerns from flaming combustion as well. This is also the concern for keeping the gases in a room or volume containing the cells below a flammability limit. Both simulations produced the same amount of gases, but non-DLM simulations showed this gas being produced more quickly.

The estimated venting times with and without the DLM are shown in Fig. 9(a) and Fig. 9(b). Figure 9(a) shows that venting times estimated from the DLM simulations are very close to the venting times estimated in the experiment [13] and that is for all N values. No significant change was seen in the venting time estimates when $N > 30$. This figure also shows that for specific N as the cell number in the array increases the venting time also

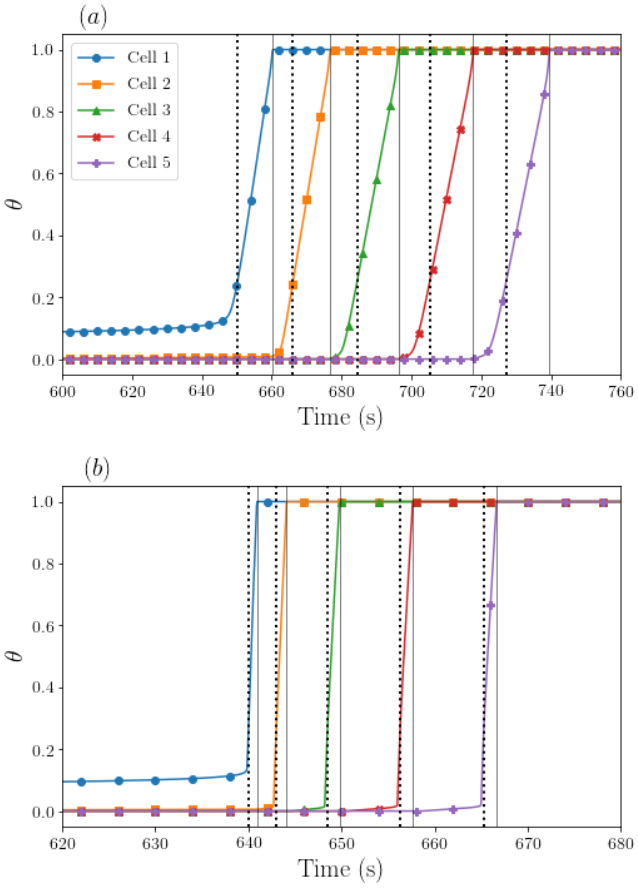

FIGURE 7. Progress variable for $N = 90$ and $\Delta t = 0.001$ for five-cell array, (a) with the DLM, and (b) without the DLM. The Dashed and solid lines indicate the start and the end of the estimated by the progress variable approach, respectively.

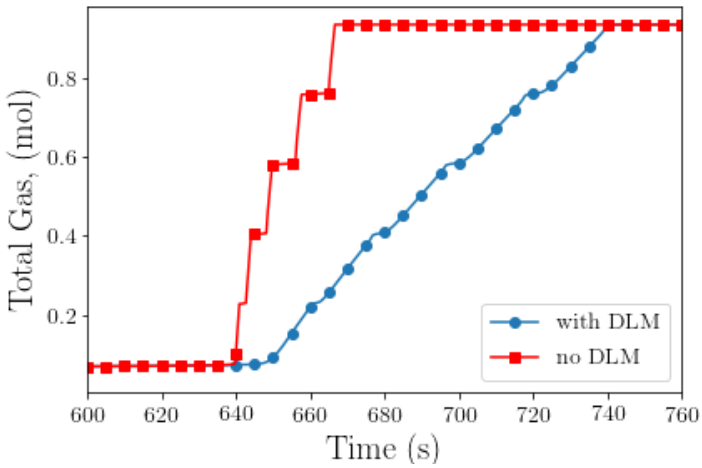

FIGURE 8. Total gas produced for $N = 90$ and $\Delta t = 0.001$ for five-cell array, (a) with the DLM, and (b) without the DLM.

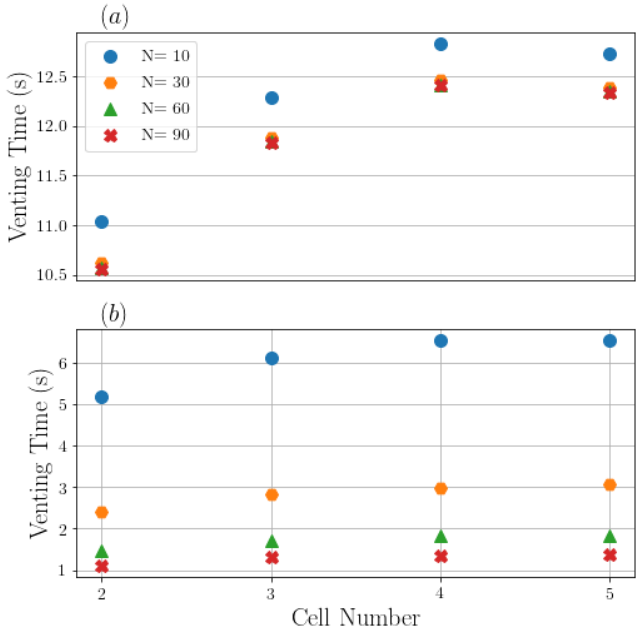

FIGURE 9. Venting time estimated using progress variable (a) with the DLM, and (b) without the DLM for $N = 10$, 30, 60, and 90 for $\Delta t = 0.001$ for five-cell array.

increases, except for the last cell, likely because of the additional heat lost to the insulation by conduction. However, Ref. [13] estimated same average venting time value for all cells in the array. For non-DLM case, Figure 9(b) shows clearly that the estimated venting times are smaller than the experimental values in Ref. [13]. Similar to simulations with the DLM, venting time decrease as N increases, and increases as cell number increases. In contrast to the DLM simulations, there is an obvious difference between the venting time values with changing N. In general, the venting times estimated from the DLM cases are higher than the values estimated form non-DLM cases and that is because the simulation becomes diffusion-controlled when the DLM is activated.

Estimated preheating times are shown in Fig. 10(a) and Fig. 10(b) for DLM and non- DLM simulations. In general and similar to venting times, the preheating time estimated using the DLM is higher than those estimated by non-DLM simulations. For DLM simulations and from Fig. 10(a), as N increases the estimated preheating times decrease as a general trend, with almost same values for $N > 30$ similar to venting times trend in Fig. 9(a). For non-DLM cases, there is slight fluctuation in preheating times with N as it is shown in Fig. 10(b). However, we can say that as N increases venting time decreases, generally. Figure 10(a) and Figure 10(b) show that for certain N as cell number in-

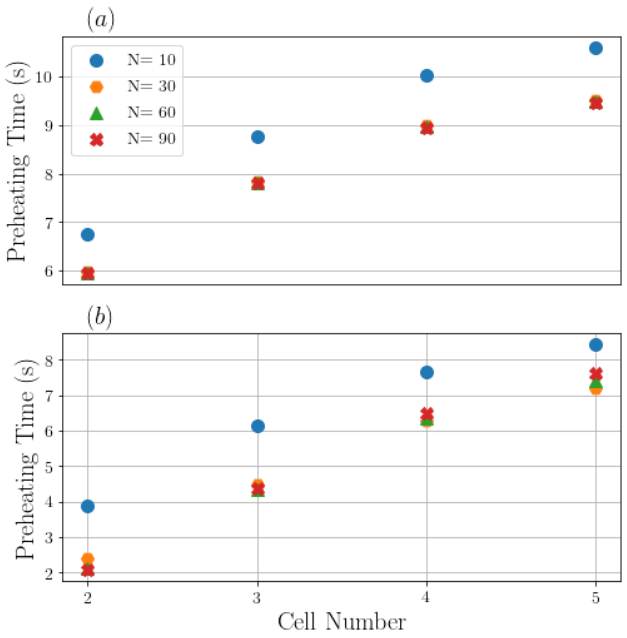

FIGURE 10. Preheating time estimated using progress variable (a) with the DLM, and (b) without the DLM for $N = 10$, 30, 60, and 90 for $\Delta t = 0.001$ for five-cell array.

creases the preheating time increases, while constant preheating time of about 4 s found in Ref. [13].

In summary for the array simulations, the progress variable approach was used to estimate the venting and preheating times. Two parameters were considered: the simulation spatial resolution, and use of the DLM. The DLM made the thermal runaway propagation slower which led to better estimation of venting times, close to the experimental values, while the preheating time values were higher than the measured ones. For DLM, in general, higher N led to better estimation of venting and preheating times.

4 Conclusion

This work undertakes a parametric study of simulation parameters in LIM1TR to establish useful guidelines for the emulation of various thermal runaway scenarios. Of particular importance to this work was matching the characteristics of vented gas products to experimental results, such as the venting time and quantity of vented products, which will be important to identify hazards associated with these combustible products.

The sensitivity study for time step (Δt) and spatial resolution (N) on estimating venting times shows that the time step has no effect on the venting times; this insensitivity to the time step is likely a result of the operator splitting and sub-cycling the stiff chemistry within the split time step. This time step refers to the operator splitting between the heat transfer and chemical source. On the other hand, the spatial discretization holds a significant effect. The importance of accurately estimating venting times comes from its relation to calculating the average venting speed from failed cells. This speed is related to Reynolds number which is a critical parameter in calculated the Nusselt number and heat fluxes from impinging jets which represent the vented gases in this case. The best predictions for cell-to-cell thermal runaway and venting were obtained with the intra-particle diffusion limiter (DLM), and this is recommended for large-scale array propagation events which represents actual scenarios of EES.

After validating the quantity of vented gas produced for the single cell, the evolution of gas products with time of the array propagation during thermal runaway was calculated. The amount of vented gases is important since knowing the amount of these gases enables us to calculate the lower flammability limit. It is desirable to remain below this level for fire safety purposes. This can also be used to estimate the minimum amount of cooling air needed to dilute the gases without causing undesired combustion.

This work shows the capability of LIM1TR to model vented gases during thermal runaway and capture their main characteristics, provides sensitivity study of important parameters in emulating different possible thermal runaway scenarios, this study can be used as guidelines for LIM1TR users. However, there are some differences that need further investigation. Future works will use the characteristics of vented gases to estimate heat transfer from these gases to other parts of an ESS for different cases.

Acknowledgements

This work was supported by the US Department of Energy, Office of Electricity, Energy Storage Program under the guidance of Dr. Imre Gyuk. This manuscript has been authored by National Technology Engineering Solutions of Sandia, LLC. under Contract No. DE-NA0003525 with the U.S. Department of Energy/National Nuclear Security Administration. The United States Government retains and the publisher, by accepting the article for publication, acknowledges that the United States Government retains a non-exclusive, paid-up, irrevocable, worldwide license to publish or reproduce the published form of this manuscript, or allow others to do so, for United States Government purposes.

REFERENCES

[1] Diaz, L. B., He, X., Hu, Z., Restuccia, F., Marinescu, M., Barreras, J. V., Patel, Y., Offer, G., and Rein, G., 2020. "Meta-review of fire safety of lithium-ion batteries: Industry challenges and research contributions". *Journal of The Electrochemical Society,* ***167***(9), p. 090559.

[2] Ouyang, D., Chen, M., Huang, Q., Weng, J., Wang, Z., and Wang, J., 2019. "A review on the thermal hazards of the lithium-ion battery and the corresponding countermeasures". *Applied Sciences,* ***9***(12), p. 2483.

[3] Feng, X., Ouyang, M., Liu, X., Lu, L., Xia, Y., and He, X., 2018. "Thermal runaway mechanism of lithium ion battery for electric vehicles: A review". *Energy Storage Materials,* ***10***, pp. 246–267.

[4] Blum, A. F., and Long Jr, R. T., 2016. *Fire Hazard Assessment of Lithium Ion Battery Energy Storage Systems*. SpringerBriefs in Fire. Springer, New York.

[5] Dispute erupts over what sparked an explosive li-ion energy storage accident. URL `https://spectrum.ieee.org/dispute-erupts-over-what-sparked-an-explosive-liion-energy-storage-accident`.

[6] Battery modules "overheat" at vistra's moss landing energy storage facility. URL `https://kion546.com/news/local-news/top-stories/2021/09/06/battery-modules-overheat-at-vistras-moss-landing-energy-storage-facility/`.

[7] Fires raise concern over energy storage battery safety in south korea. URL `https://www.infolink-group.com/en/storage/energy-storage-market-trends/fires-raise-concern-over-energy-storage-battery-safety-in-south-korea`.

[8] Lamb, J., Orendorff, C. J., Steele, L. A. M., and Spangler, S. W., 2015. "Failure propagation in multi-cell lithium ion batteries". *Journal of Power Sources,* ***283***, pp. 517–523.

[9] Torres-Castro, L., Kurzawski, A., Hewson, J., and Lamb, J., 2020. "Passive mitigation of cascading propagation in multi-cell lithium ion batteries". *Journal of The Electrochemical Society,* ***167***(9), p. 090515.

[10] Li, Q., Yang, C., Santhanagopalan, S., Smith, K., Lamb, J., Steele, L. A., and Torres-Castro, L., 2019. "Numerical investigation of thermal runaway mitigation through a passive thermal management system". *Journal of Power Sources,* ***429***, pp. 80–88.

[11] Feng, X., He, X., Ouyang, M., Lu, L., Wu, P., Kulp, C., and Prasser, S., 2015. "Thermal runaway propagation model for designing a safer battery pack with 25 ah linixcoymnzo2 large format lithium ion battery". *Applied energy,* ***154***, pp. 74–91.

[12] Feng, X., Lu, L., Ouyang, M., Li, J., and He, X., 2016. "A 3d thermal runaway propagation model for a large format lithium ion battery module". *Energy,* ***115***, pp. 194–208.

[13] Archibald, E., Kennedy, R., Marr, K., Jeevarajan, J., and Ezekoye, O., 2020. "Characterization of thermally induced runaway in pouch cells for propagation". *Fire technology,* ***56***(6), pp. 2467–2490.

[14] Kurzawski, A., and Shurtz, R., 2019. LIM1TR: Lithium-ion Modeling with 1-D Thermal Runaway v1.0. Tech. Rep. SAND2021-12281, Sandia National Lab, (SNL-NM), Albuquerque, NM (United States).

[15] Kurzawski, A. Lim1tr: Lithium-ion modeling with 1-d thermal runaway. ULR `https://github.com/ajkur/lim1tr`.

[16] Kurzawski, A., Torres-Castro, L., Shurtz, R., Lamb, J., and Hewson, J. C., 2021. "Predicting cell-to-cell failure propagation and limits of propagation in lithium-ion cell stacks". *Proceedings of the Combustion Institute,* ***38***(3), pp. 4737–4745.

[17] Richard, M., and Dahn, J., 1999. "Accelerating rate calorimetry study on the thermal stability of lithium intercalated graphite in electrolyte. i. experimental". *Journal of The Electrochemical Society,* ***146***(6), p. 2068.

[18] Shurtz, R. C., Engerer, J. D., and Hewson, J. C., 2018. "Predicting high-temperature decomposition of lithiated graphite: Part i. review of phenomena and a comprehensive model". *Journal of the Electrochemical Society,* ***165***(16), p. A3878.

[19] Shurtz, R. C., Engerer, J. D., and Hewson, J. C., 2018. "Predicting high-temperature decomposition of lithiated graphite: Part ii. passivation layer evolution and the role of surface area". *Journal of the Electrochemical Society,* ***165***(16), p. A3891.

[20] MacNeil, D., and Dahn, J. R., 2002. "The reactions of li0. 5coo2 with nonaqueous solvents at elevated temperatures". *Journal of The electrochemical society,* ***149***(7), p. A912.

[21] Shurtz, R. C., and Hewson, J. C., 2020. "Materials science predictions of thermal runaway in layered metal-oxide cathodes: A review of thermodynamics". *Journal of The Electrochemical Society,* ***167***(9), p. 090543.

[22] Shurtz, R. C., 2020. "A thermodynamic reassessment of lithium-ion battery cathode calorimetry". *Journal of the Electrochemical Society,* ***167***(14), p. 140544.

[23] Coman, P. T., Rayman, S., and White, R. E., 2016. "A lumped model of venting during thermal runaway in a cylindrical lithium cobalt oxide lithium-ion cell". *Journal of Power Sources,* ***307***, pp. 56–62.

[24] Walker, R., and Pavía, S., 2015. "Thermal performance of a selection of insulation materials suitable for historic buildings". *Building and environment,* ***94***, pp. 155–165.

[25] Baird, A. R., Archibald, E. J., Marr, K. C., and Ezekoye, O. A., 2020. "Explosion hazards from lithium-ion battery vent gas". *Journal of Power Sources,* ***446***, p. 227257.